

FLEXSTAGE: LIGHTWEIGHT MAGNETICALLY LEVITATED PRECISION STAGE WITH OVER-ACTUATION TOWARDS HIGH-THROUGHPUT IC MANUFACTURING*

Jingjie Wu and Lei Zhou

Department of Mechanical Engineering
University of Wisconsin-Madison, WI, USA

INTRODUCTION

Precision motion stages play a critical role in various manufacturing and inspection equipment, for example, the wafer/reticle scanning in photolithography scanners and positioning stages in wafer inspection systems. To meet the growing demand for higher throughput in chip manufacturing and inspection, it is critical to create new precision motion stages with higher acceleration capability with high control bandwidth [1], which calls for the development of lightweight precision stages. However, in today's precision motion systems, only the rigid body motion of the system are under control, and the flexible dynamic systems are in open loop. For these systems, the motion control bandwidth is limited by the first structural resonance frequency of the stage, which enforces a fundamental trade-off between the stage's bandwidth and acceleration capability, as is shown in Fig. 1.

Aiming to overcome this trade-off, we have introduced a sequential structure and control design framework for lightweight stages with the low-frequency flexible modes of the stage are under active control [2]. To facilitate the controller design, we further propose to **minimize** the resonance frequency of the stage's mode being controlled and to **maximize** the resonance frequency of the uncontrolled mode. The system's control bandwidth is placed in between the resonance frequencies, as shown in Fig. 2. Such an optimization process can enforce material removal in the stage's structure to allow for compliance in the actively-controlled flexible modes, and add material to stiffen the uncontrolled modes.

This abstract presents the design, optimization, building, and experimental evaluations for a lightweight magnetically levitated planar stage, which we call Flexstage, with first flexible mode actively controlled via over-actuation. The stage's structure is designed with intentionally introduced

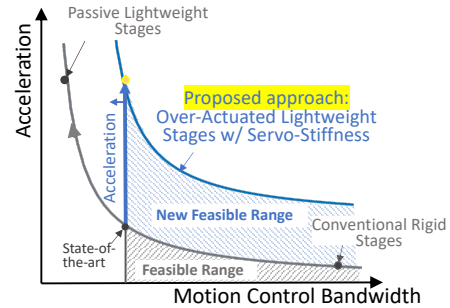


FIGURE 1. Acceleration-bandwidth trade-off in today's precision positioning systems and motivation for the proposed method.

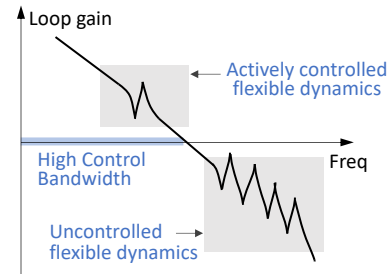


FIGURE 2. Illustration of the proposed lightweight stage design with active flexible mode control.

compliance to facilitate the flexible mode control and to reduce moving weight. Simulations show the proposed design is highly promising in enabling stages with lightweight without sacrificing control bandwidth. We have some preliminary results now and are still working on the experimental evaluations for the closed-loop system, and will present the results in the oral presentation.

STAGE DESIGN OPTIMIZATION

Figure 3a shows the structural design for the moving stage considered in this work, which is a rib-reinforced structure made of 7075-T6 aluminum alloy of 300 mm \times 300 mm in size. There are four neodymium permanent magnet arrays of 70 mm \times 70 mm \times 6.35 mm arranged at the corners of the stage to provide both the thrust forces

*ACCEPTED FOR ASPE 38TH ANNUAL MEETING

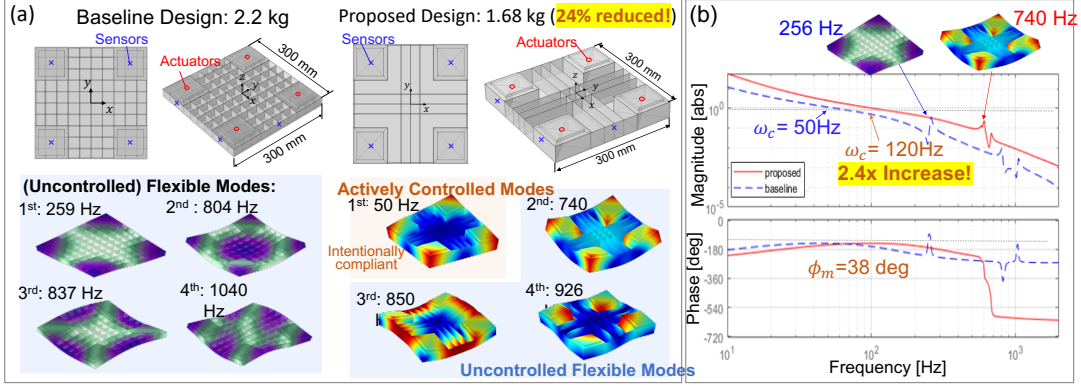


FIGURE 3. (a) Proposed and baseline moving stages structure design. Note that the proposed case has one flexible mode with intentionally introduced compliance. (b) Comparison of loop gains of the proposed and baseline design in scanning direction.

for planar motion and the levitation forces. To reduce the stage's weight and have the first low-frequency flexible mode actively controlled, the stage's geometry can be determined by the following optimization problem:

$$\begin{aligned}
 \min_{\theta_p} \quad & J_m(\theta_p), \\
 \text{s.t.} \quad & \omega_i \leq \omega_{low}, \quad i = 1, \dots, n \\
 & \omega_j \geq \omega_{high}, \quad j = n + 1, \dots, m \\
 & \theta_{p,min} \leq \theta_p \leq \theta_{p,max}.
 \end{aligned} \quad (1)$$

Here, the objective function J_m is the stage's weight, θ_p represents the vector for the stage's geometric parameters, ω_i is the i -th resonance frequency with its corresponding mode shapes actively controlled, and ω_j is the j -th modal frequency with corresponding vibration modes not controlled. ω_{low} is the upper bound for the actively-controlled modal frequencies, and ω_{high} is the lower bound for the uncontrolled modal frequencies. $\theta_{p,min}$ and $\theta_{p,max}$ are the lower and upper bounds for the stage's geometric parameter, respectively. By solving this optimization program, the material of the stage is partially removed to allow for compliance in the actively controlled flexible modes while the material kept can stiffen the uncontrolled modes. Here, ω_{low} is chosen to be 50 Hz so that the control bandwidth can crossover well beyond it and ω_{high} is 560 Hz from sweeping to minimize the stage's weight and the limitation on achievable control bandwidth. The first four vibration mode shapes and corresponding resonance frequencies of the optimal stage structure are shown in Fig. 3a. For comparison, a baseline stage structure in Fig. 3 is designed to constrain the first resonance frequency above 250 Hz with a target bandwidth of 50 Hz.

ACTUATOR AND SENSOR PLACEMENT

With the optimal stage's structure from (1), the actuator and sensor placement optimization problem with first several flexible modes actively controlled can be formulated as

$$\max_{\theta_a \in D_a} J_a(\theta_a) = \sum_{i=1, \dots, n} W_{pi}(\theta_a) - \gamma \sum_{i=n+1, \dots, m} W_{pi}(\theta_a), \quad (2)$$

$$\max_{\theta_s \in D_s} J_o(\theta_s) = \sum_{i=1, \dots, n} W_{oi}(\theta_s) - \gamma \sum_{i=n+1, \dots, m} W_{oi}(\theta_s), \quad (3)$$

where θ_a and θ_s are vectors of actuator and sensor placement parameters, respectively; D_a and D_s are the design feasible domains for actuator/sensor locations, and γ is a positive user-defined weighting constant. W_{pi} and W_{oi} are the controllability and observability grammians of i -th flexible mode, respectively, which can be calculated as

$$W_{pi} = \frac{\|\phi_i(\theta_a)^\top B_a(\theta_a)\|_2^2}{4\zeta_i\omega_i}, \quad (4)$$

$$W_{oi} = \frac{\|C_s(\theta_s)^\top \phi_i(\theta_s)\|_2^2}{4\zeta_i\omega_i}, \quad (5)$$

where ϕ_i is the mass-normalized mode shape of i -th flexible mode, B_a and C_s are the force and measurement assembling matrices, ζ_i is the modal damping ratio, and ω_i is the i -th resonance's natural frequency. The controllability/observability grammians W_{pi} and W_{oi} quantitatively represent the controllability/observability of the corresponding flexible mode, reflecting on its peak resonance magnitude in the system's frequency response.

With actuator/sensor placement optimization in (2) and (3), our goal is to maximize the controllability/observability for the actively-controlled

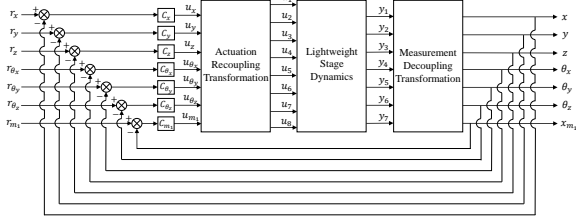


FIGURE 4. Control block diagram for the lightweight precision positioning stage with model decoupling.

modes to lower the required controller gain, and to minimize those of the uncontrolled modes to mitigate their coupling effect in the control systems and thus facilitate the controller design. It is worth noting such trade-off between the two design goals is determined by the value of weighting parameter γ as: a low value in γ emphasizes reducing the needed control effort for actively-controlled modes, and a high value in γ emphasizes reducing the cross-talk between uncontrolled modes and controlled modes for higher control bandwidth. For the baseline case, we do not apply such placement optimization.

FEEDBACK CONTROL DESIGN

After the stage's hardware design (including both stage's structure and actuator/sensor placement) is optimized, the plant dynamic model can be derived. Finally, feedback controllers are designed for each motion axis to attain the target closed-loop control performance. Figure 4 shows a block diagram for the closed-loop system with all six rigid-body DOFs and one flexible mode of the lightweight stage under active control. Here, the lightweight stage plant dynamics $P : u \rightarrow y$ can be obtained after solving (1), (2), and (3). The actuator control inputs u and the sensor measurements y are recoupled and decoupled by transformation matrices, respectively, to obtain decoupled system DOFs. Seven single-input, single-output (SISO) feedback controllers can then be synthesized for the seven decoupled channels assuming the cross-talk between different channels is negligible near the target control bandwidth. For each DOF, a fixed-structure SISO controller is selected as [3]

$$C_k(s) = K_p \left(\frac{s + \omega_i}{s} \right) \left(\frac{s}{\omega_d} + 1 \right) \left(\frac{\omega_{lp}^2}{s^2 + 2z_{lp}\omega_{lp}s + \omega_{lp}^2} \right), \quad (6)$$

where the controller parameters are described in Table 1. This controller design significantly facilitates the parameter tuning process since all the controller parameters except the controller gain

TABLE 1. Controller parameters [4].

Parameter	Description	Typical Value
ω_{bw}	Desired bandwidth [rad/s]	—
α	PID frequency ratio	3
K_p	Proportional gain	—
ω_i	Integrator frequency	ω_{bw}/α^2
ω_d	Differentiator frequency	ω_{bw}/α
ω_{lp}	Lowpass filter frequency	$\alpha\omega_{bw}$
z_{lp}	Lowpass filter damping ratio	0.7

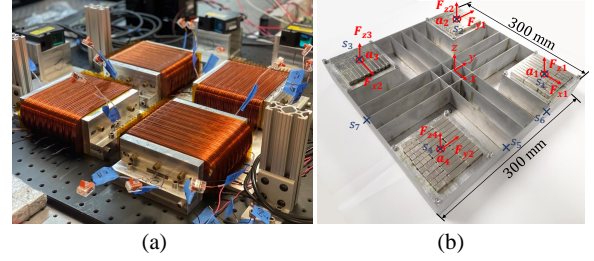


FIGURE 5. (a) Stator assembly (b) Fabricated stage with forces location and directions labeled

can all be determined by a single parameter, desired bandwidth ω_{bw} [4]. The proportional gain K_p and the target bandwidth are chosen such that the control bandwidth is maximized for each channel while satisfying a robustness criteria [5]

$$\|S_k(s)\|_\infty \leq 2, k = 1, \dots, n, \quad (7)$$

where $S_k(s)$ is the closed-loop sensitivity function of the k -th channel as $S_k = (I - G_k C_k)^{-1}$.

This PID controller structure is also used in the baseline case and tuned to achieve its target bandwidth. Fig. 3b illustrates the loop gains of both proposed and baseline designs in y -DOFs, the performance of which are most critical. It can be observed that with sufficient stability margins in both cases, the control bandwidth in proposed design is significantly larger than the baseline design. The weight of the proposed stage design (1.68 kg) is reduced by 24% compared to baseline design (2.21 kg). The comparisons demonstrate the potential of the proposed framework to improve the stage's acceleration capability while maintaining high bandwidth and robustness.

PROTOTYPE INTRODUCTION

To verify the improvement in overall system performance, the optimized stage is fabricated as shown in Fig. 5b. The magnet arrays at corners to provide thrust and levitation force are made of N52 NdFeB and have the pattern of a traditional 4-segment-per-spatial-period Halbach array, which can generate a higher magnetic field.

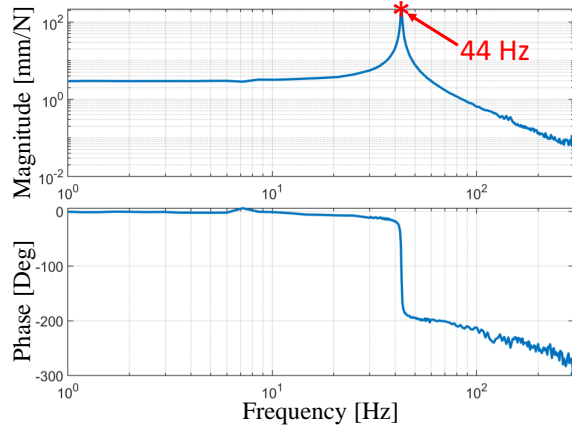


FIGURE 7. Identified 7th channel plant frequency response.

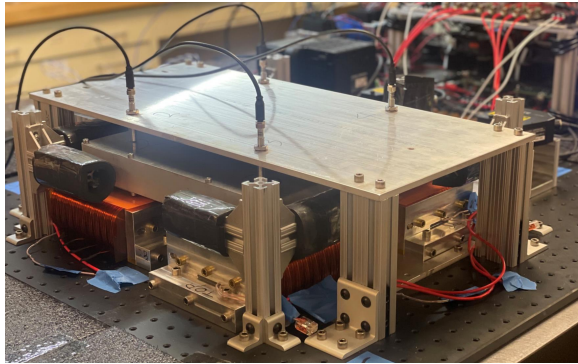


FIGURE 8. Experimental Setup.

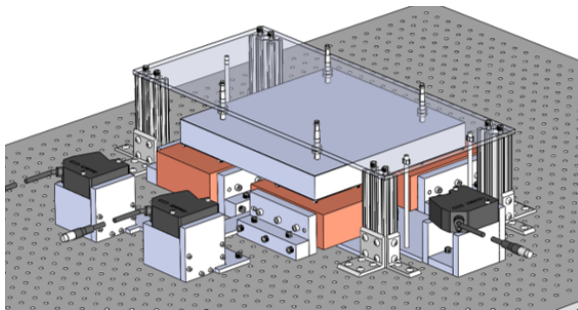


FIGURE 6. Planar motor hardware CAD model for experimental evaluation.

Fig. 5a shows the assembly of the four stators holding coil windings with the thickness being 15 mm according to parameter sweeping in the Ansys Maxwell electromagnetic simulations to maximize the instantaneous force capability and therefore the acceleration capability. The APEX PA12 power op-amp is used inside of a customized current controller with a bandwidth of around 5kHz to provide the current for the coils up to 10 A. Each coil consists of 100 turns of AWG#19 to have sufficiently small resistance and thus provide the de-

sired peak current. The overall planar motor CAD design for actuation and sensing of the stage is shown in Fig. 6 including four DW-AS-509-M8-390 inductive sensors to measure the vertical displacement and three LK-H152 laser displacement sensors to measure full x and y axis motion. The experimental setup of the whole planar motor is shown in Fig. 8.

As a primary test of the planar motor system, we employ a lead-lag form PID controller for each motion axis and then tune all the controller parameters to only stabilize the closed-loop system. Then we perform a system identification for each DOF's transfer function by Dynamic Signal Analyzer to validate the stage's mass, mode shapes, and resonance frequencies derived from COMSOL Finite Element simulation. Fig. 7 shows the identified frequency response of the 7th channel for the first mode being actively controlled. The 1st resonance frequency of the fabricated stage structure is 44Hz, which well matches with our prediction. We are currently working on further system identification and tune the controllers to obtain a high control bandwidth, and the results will be presented at the conference and our future works.

REFERENCES

- [1] Oomen T, van Herpen R, Quist S, van de Wal M, Bosgra O, Steinbuch M. Connecting system identification and robust control for next-generation motion control of a wafer stage. *IEEE Trans on Ctrl Sys Tech.* 2013;22(1):102–118.
- [2] Wu J, Zhou L. Transcending the Acceleration-Bandwidth Trade-off: Lightweight Precision Stages with Active Control of Flexible Dynamics. In: 37th ASPE Annual meeting. ASPE; 2022. .
- [3] Franklin GF, Powell JD, Emami-Naeini A, Powell JD. *Feedback control of dynamic systems.* vol. 4. Prentice hall Upper Saddle River; 2002.
- [4] Butler H. Position control in lithographic equipment [applications of control]. *IEEE Control Sys Mag.* 2011;31(5):28–47.
- [5] Ortega M, Rubio F. Systematic design of weighting matrices for the H mixed sensitivity problem. *Journal of Process Control.* 2004;14(1):89–98.